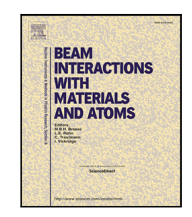
Contents lists available at ScienceDirect

## Nuclear Inst. and Methods in Physics Research, B

journal homepage: www.elsevier.com/locate/nimb





# Improvements for heavy-ion accelerator mass spectrometry at the university of Notre Dame's nuclear science laboratory

Adam M. Clark\*, Austin D. Nelson, Thomas L. Bailey, Lauren K. Callahan, Adam Mazurek, Philippe Collon

Department of Physics and Astronomy, University of Notre Dame, Notre Dame, IN 46556, United States

#### ARTICLE INFO

Keywords: AMS Uranium Iodine Gas ionization detector Time-of-flight

#### ABSTRACT

The detection of heavy (A > 127), long-lived trace radionuclides using accelerator mass spectrometry requires accelerator systems with high mass resolution and detectors with high efficiency, timing and energy resolution, and resistance to degradation. At the University of Notre Dame's Nuclear Science Laboratory, a two-anode gas ionization detector, similar to others employed at ETH Zurich, Vienna, and the Australia National University, has been built to be used with a time-of-flight system. This new detector is more robust than the existing Si detector, with two high resolution  $\Delta E$  segments. This work describes the detector design and modifications to the time-of-flight system, summarizes the observed performance, and provides comparisons to a Geant4 model. The energy resolution (9% for 44 MeV  $^{238}$ U beams) was found to be better than the existing Si detector and its larger acceptance contributed a factor of five improvement (from 4% to 20%) in transmission through the detection system for uranium beams.

## 1. Introduction

Signatures of select heavy radionuclides in the environment (e.g. 129 I, 233, 236 U, 237 Np, and 239, 240, 244 Pu) are in many cases found to be orders of magnitude higher than the expected natural production. The observed excess of these nuclides are typically due to anthropogenic sources such as nuclear reprocessing and fallout [1-4]. Their detection, even down to ultra-low levels, serve as useful environmental tracers and is applicable to nuclear forensics. However, recent observations have also been attributed to stellar production and deposition (i.e. from near-by supernovae or kilonovae). Stellar <sup>244</sup>Pu, which is produced exclusively by the astrophysical rapid neutron capture process (r process), has been detected alongside the now well-known signal of 60Fe (produced via the slow neutron capture process) [5]. Projections of this detection have been extended. If <sup>244</sup>Pu is created and deposited on Earth, then other radionuclides, such as  $^{93}\mathrm{Zr},^{129}\mathrm{I},^{182}\mathrm{Hf},$  as well as other actinide isotopes such as  $^{237}\mathrm{Np}$  and <sup>247</sup>Cm, must be as well [6]. Further searches for these isotopes in deepsea crusts, meteorites, and even lunar material could assist to shed light on these production events. The importance of these studies has encouraged the development of Accelerator Mass Spectrometry (AMS) capabilities for heavy ions at the University of Notre Dame's Nuclear Science Laboratory (NSL).

At the NSL, one beamline is dedicated to systems required for AMS measurements. A  $2.51\ m$  time-of-flight system was implemented

In order to increase both the transport efficiency and radiation hardness of the system, thinner carbon foils ( $\sim$ 3  $\mu g/cm^2$ ) were used with the MCP's and a compact ionization chamber (IC) was built to be used in place of the Si detector for heavy ions. The design and performance of the IC, changes to the MCP foils, and the subsequent impact on our detection system efficiency and resolution using stable or abundant ion beams are all explored in this study.

## 2. Ionization chamber design

The design of the IC replicates those used at ETH Zurich [9], the Vienna Environmental Research Accelerator (VERA) [10], and the Australian National University (ANU) [11], as those dimensions satisfy our

E-mail address: Adam.M.Clark.285@nd.edu (A.M. Clark).

and first used for  $^{129}\mathrm{I}$  measurements [7,8]. This system consists of two MicroChannel Plate (MCP) detectors which measure a pulse of secondary electrons as individual ions pass through thin carbon foils. These ions are then stopped in a Si detector for energy detection. In these initial studies, it was determined that the efficiency of the detection system was limited by transmission losses due to scatter from the thin carbon foils ( $\sim\!10~\mu\text{g/cm}^2$ ) of each MCP configuration and the small active area of the Si detector (100 mm², diameter  $\approx\!11.3$  mm). Also, it was observed that, over the course of a week of measurements, the energy resolution of the Si detector had greatly degraded, beginning with sub-5% and ending greater than 15%.

<sup>\*</sup> Corresponding author.



Fig. 1. Pictures of the internals of the ionization chamber (left) and detector body (right). The uneven wire spacing in the Frisch grid is an artifact of it being done manually and has since been improved.

spacial restrictions which require easy insertion and retraction inside of a 100 mm beamline six-way cross without breaking vacuum. Electrical diagrams, a pre-amp circuit board, and CAD drawings were generously provided by to us by ANU. While many facets of the detection system were unchanged from original designs, there are a few deviations that were made to some of the components.

The internal dimensions are unchanged from what is described in Martschini et al. 2019 [11] except for the detector window. These dimensions are described in the sentences that follow. The anode plate is 64 mm in length and 47.5 mm in width. Anode sections were cut on a copper coated PCB board with the first anode spanning 34 mm and the second covering 30 mm to accommodate for a recessed detector window. The detector housing, which consists of a detector body and lid machined from aluminum, and the cathode, cut from a 0.2 mm stainless steel sheet, were both electrically grounded through the preamplifier board. The Frisch grid frame was made from 1 mm thick stainless steel with 1 mm spaced etches to assist in the wrapping of 20 µm diameter gold-coated tungsten wire, which was done by hand and adhered with conductive epoxy. Both anode plates were biased to +300 V and the Frisch grid was biased to +180 V via a voltage divider. The preamp board is mounted directly above the anode plate and the short Teflon-shielded wires allow for immediate amplification of the detector signal to reduce noise. Two AC-coupled CREMAT Cr-110 lownoise preamplifiers (Cremat Inc, West Newton, MA, USA) were used. The cathode to Frisch grid and Frisch grid to anode spacing is 32 mm and 6 mm respectively.

Some minor differences between this IC and the designs mentioned above include material selection. Spacing between each component was achieved with a nylon structure (rather than PEEK) composed of threaded rods, spacers, and coupling nuts. Nylon was selected over PEEK, which has been used in aforementioned versions, due to availability. Also, a custom piece was 3D printed out of PLA to provide structure and isolate the cathode from the detector housing. Fig. 1 shows a picture of the internal structure of the detector and the detector body.

The detector window consists of a 1  $\mu m$  Mylar foil. Mylar was selected due to availability, while the thickness was chosen for its strength over a 20 mm diameter opening while maintaining a sufficient burst pressure. The original window mounts were designed to recess into the detector region such that ions pass through the window directly into the active region (see Fig. 2). However, vacuum pressures exceeded  $10^{-5}$  Torr in the region of the nearest MCP, likely due to micro-tears in the mylar sheet. Therefore, the retracted window mount was replaced with a simple aluminum plate with a 20 mm diameter hole and the window was sealed by compression on the O-ring surface. A comparison



Fig. 2. Recessed detector window (left) and non-recessed window (right). The recessed window is by design and will be pursued in future work while satisfying vacuum requirements. A non-recessed solution was used for this study and was compressed by a simple flat plate.

of the recessed window and the non-recessed configuration are shown in Fig. 2. This allowed for more rapid testing for leaks without the need to wait for adhesives to cure. Once new window material is acquired, the original mounting configuration will be pursued. Since the window was not recessed, there was an extra 14 mm region between the window and the first anode, which resulted in energy loss which is not measured by the anodes and greatly contributed to the broadening of the energy resolution.

The detector was mounted on a UHV Pneumatic Linear Shift Mechanism (LSM38-150-PS) by means of a 1/2 inch diameter hollow stainlesssteel supporting rod. An image of this mechanism is shown in Fig. 3 as seen on the beamline. An insulating adaption piece made from Delrin<sup>®</sup> joins the detector housing to the supporting rod. This ensured that the detector body is electrically isolated through the preamplifier ground and not to the beamline ground. Signals from the board were run up the length of the supporting rod via a Teflon-coated ribbon cable and fed-out through a 15-pin connector. An external cable connected the 15-pin connector to a NIM module made in-house to feed-in the detector bias and provide a test port for a pulser, as well as feed-out the temperature readout and anode output signals via BNC connectors. The anode signals were further amplified with Ortec model 572 amplifiers. The detector gas was controlled by a gas-handling system. Isobutane was fed-in at the top of the linear shift mechanism and flowed down the supporting rod into the detector volume.



Fig. 3. Linear motion device used to move and hold the detector. Supply and return gas lines (top left) run to a gas handling system and a 15-pin connector (top right) provides the interface to the detector electronics.

#### 3. AMS beamline

The newly constructed IC was added to the AMS beamline at the NSL in December 2021. Following the retractable time-of-flight system, the detector is one of three insertable detection devices on a six-way 100-mm Dependex cross, the others being a Si detector (100 mm<sup>2</sup> active area) with a built-in 9 mm diameter aperture and a Faraday cup.

#### 3.1. Time-of-flight system

At the NSL, a dual MCP configuration was installed for the detection of heavy ions [7,8]. These MCPs were generously provided to us by Michael Paul from the Racah Institute of Physics of the Hebrew University of Jerusalem and were implemented in reverse order and separated by a greater distance (1.43 m compared to 2.51 m at the NSL) than described in Berkovits et al. 2000 [12]. The present layout of the AMS beamline is depicted in Fig. 4. It is shown that two distinct MCP detector configurations being used. The first, referred to as the 90° MCP, has a carbon foil whose surface is perpendicular to the

incoming beam and uses a set of grids as an electrostatic mirror to redirect electrons emitted from particles passing through the foil to the detector. Each grid is composed of 20  $\mu m$  gold-tungsten wire, which was hand-wrapped with a spacing of 1 mm. The second, referred to as the 45° MCP, has a carbon foil oriented at 45° with respect to beam and relies on direct back-scattered electrons into the MCP detector. Initially, the 45° MCP was rotated 180° and forward scattered electrons were used for detection. It was observed, however, that scattered ions from the 90° MCP had a direct path to the angled MCP and led to an additional time-of-flight peak when the spectrum was not gated for energy detection. This rotation has had no observable impact on detection, other than the removal of the additional peak.

Signals from the MCPs are processed through a constant fraction discriminator (Ortec 935 Quad CFD). The 45° MCP was used as the "start" detector of the data acquisition (DAQ) system and the 90° MPC was used as the "stop" signal by first passing through physical delay lines prior to being sent into the time-to-digital converter (TDC). This reversal of the assigned start and stop signal reduces the dead-time by triggering the DAQ only if both signals for time-of-flight are observed. In previous experiments, it was observed that the timing resolution from this system was more than sufficient for  $^{129}$ I measurements. However, the detection system transmission efficiency was lower than anticipated ( $\sim$  60% compared to 21% which was observed).

Efficiency losses of the time-of-flight system are comprised of the following components: (1.) Masking due to the grid wires critical to the support of the thin carbon foils and the wires composing the grid mirror. We calculate that the maximal detection efficiency due to the grid masking alone was 86%. (2.) Transmission losses due to beam scatter from the thin carbon foils required for the timing detection. The main cause is the angular straggling from this interaction, which is exacerbated by a collodion coating, resulting in an increased beam size at the second carbon foil frame and detector window. In order to improve the transmission, we installed thinner foils and chose a larger frame for the 45° MCP. The system, described as before and after these changes define the two test configurations below.

#### 3.1.1. Tested configurations

In order to demonstrate improvements to particle transmission through the detector system, two distinct configurations were compared. The first consisted of an 18 mm diameter  $90^\circ$  foil frame followed by a 12 mm diameter foil frame at  $45^\circ$  and a  $100~mm^2$  Si detector with a 9 mm tantalum aperture. This configuration was used prior to the completion of the IC. The foils for the MCPs were 9.6 and  $10~\mu g/cm^2$  respectively. The second configuration also used an 18 mm  $90^\circ$  foil frame but was instead followed by an 18 mm foil frame at  $45^\circ$  and the new IC described in Section 2. Simultaneously, both foils were replaced with thinner foils ( $\sim 3~\mu g/cm^2$ ) to reduce angular scattering. To understand the effects of scattering and subsequent losses due to beam size, these configurations were simulated and compared to experimental data.

#### 4. Geant4 simulation

To assist in a detailed characterization of limitations in the time-offlight system's efficiency, a Geant4 simulation was created to identify areas of improvement and predict an impact on the transmission efficiency. A recent study by Zheng et al. demonstrated consistency between data and simulation using this method [13].

The beam was input as a Gaussian energy distribution with  $\sigma$ =20 keV and was simulated spatially both as an ideal "pencil" beam and a uniform circular distribution with a diameter of 9 mm starting just before the first MCP. The size, which is considered large, was a compromise as it was observed that uranium was not able to be focused down to completely pass through the 7.5 mm aperture (see Fig. 4) while tuning to the last Faraday cup. Simultaneously, there was no detectable difference between the rate on the 90° MCP, which is believed to

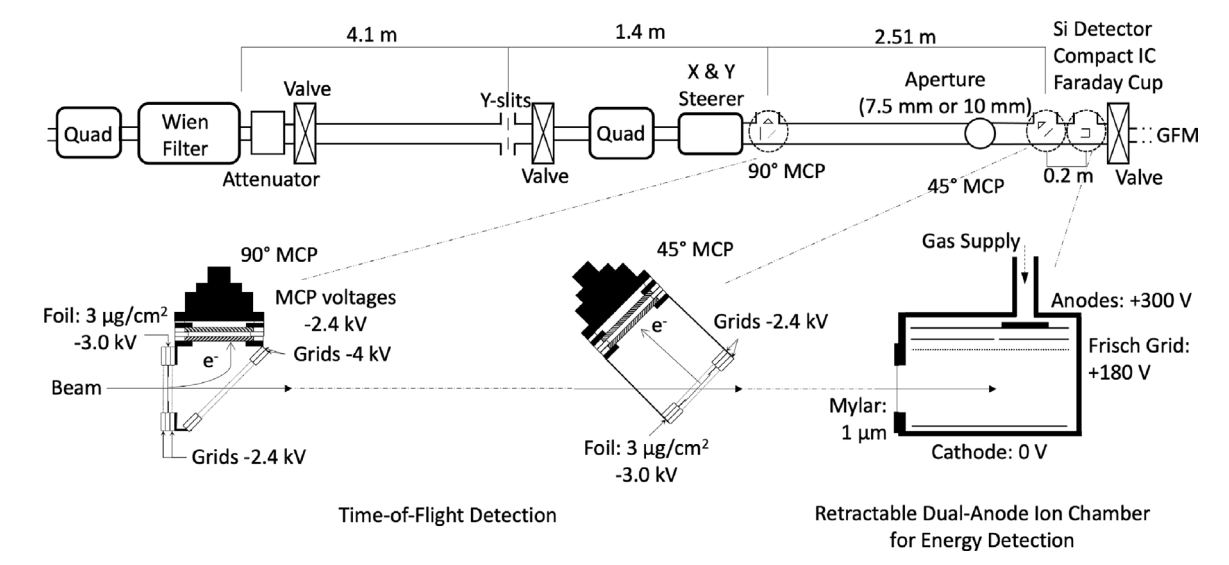


Fig. 4. The AMS beamline, highlighting the location of critical components prior to a Gas-Filled Magnet. Distances are not depicted to scale but notable distances are listed. The schematic here of the IC is depicted with a recessed window, but for spectra presented in this work the window was not recessed.

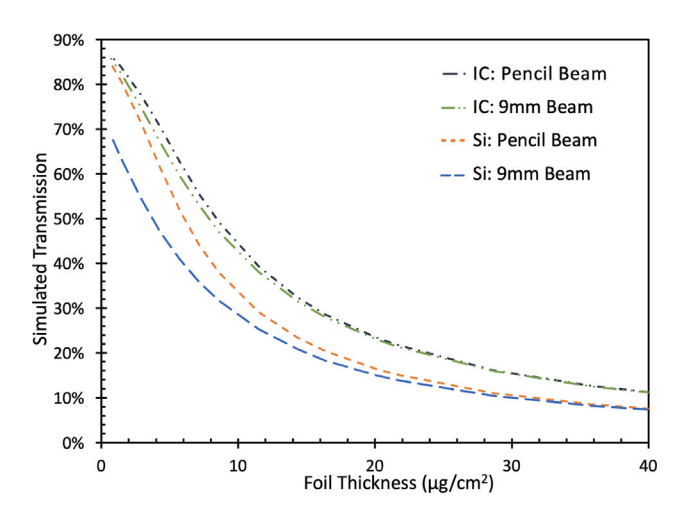


Fig. 5. Geant4 predictions of the particle transmission from the 90° MCP to the energy detector (either Si or new IC) for the two test configurations as a function of the thickness of the 90° MCP foil for the specific case of a 44 MeV  $^{238}$ U beam. The assumed thickness for the 45° MCP foil for this simulation was 10  $\mu g/cm^2$ . Due to the acceptance of the Si detector (9 mm in diameter) being equivalent to the projected beam size, the projected maximum transmission was not achieved due to losses from straggling by the 45° foil.

capture all of the beam since it was 18 mm in diameter, compared to the Si detector, which had an acceptance of 9 mm. Therefore, we modeled what we believe is a worse case scenario for the beam size.

The time-of-flight system was modeled using the carbon foils and foil frames. Electron drift times for both MCP configurations were assumed to be minor contributions and not present in this simulation. Scattering was simulated using the Urban multiple scattering formalism provided within the software. The foils were input as carbon and the thickness to areal density was converted assuming a density of 2.01 g/cm³ [14].

Two unique configurations reflecting the experimental conditions for tests of the detection system described in Section 3.1.1 were simulated. It was anticipated that the experimentally determined transmission would fall within limits presented by the pencil beam and 9 mm diameter parallel beam as shown in Fig. 5 which simulates this relationship for a 44 MeV  $^{238}\text{U}$  beam. This plot demonstrates that variation in the expected transmission becomes more sensitive to the

beam size as the first carbon foil thickness decreases. It was clear, and expected, that thinner carbon foils would result in higher transmission due to less angular straggling. This effect was most dramatic when the second MCP foil frame or the energy detector acceptance were small.

The IC was modeled to the same specifications described in Section 2. Energy deposited in each anode region was determined through the simulation of energy deposition within regions constrained along the beam and horizontal directions by the Frisch grid frame and vertically constrained by the Frisch grid and cathode plate. The detector gas of isobutane was scaled by pressure assuming a density of 2.51 mg/cm<sup>3</sup>. Effects for non-uniformity or bowing of the detector window, simulations of electron showers, charge collection in the IC, and resolution contributions from electronic noise are not present in this model. As a result, we anticipated that the simulated resolution would be higher than that of the physical detector. Similarly, modeling of the Si detector was defined by the 9 mm shield, a 100 nm deadlayer of Si followed by a thick Si active region. The simulation can be run both without (see Section 5.1 or with (see Section 5.2) the time-of-flight foils with very little modification.

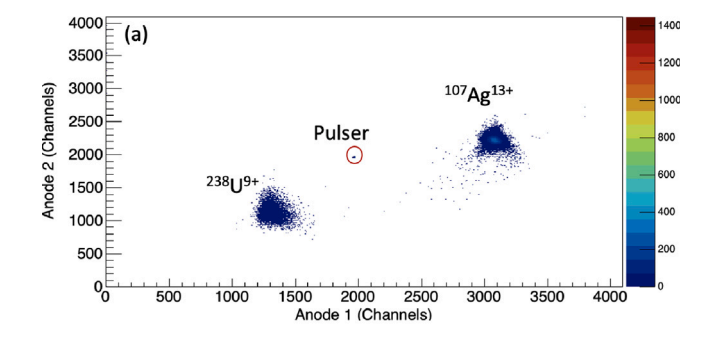
## 5. Results and discussion

In this study, the new IC was tested with and without the timeof-flight system. The data from these tests was then compared to the Geant4 simulation.

#### 5.1. Ionization chamber performance

When the IC was experimentally tested without the time-of-flight system, sub-5% energy resolution, which is defined here as the full-width at half maximum over the centroid, was achieved for the majority of the mass, energy, and detector pressure combinations. For a 44.0 MeV <sup>238</sup>U beam, the resolution ranged between 4.9% and 9.2% for pressures of 20.8 to 40 Torr of isobutane. A summary of a subset of tested beams and the observed resolutions are presented in Table 1. A spectrum of heavy ions and the determined energy resolution is shown in Fig. 6. The contribution to the energy resolution from the electronics was measured using a pulser and found to be 92 keV.

In order to observe isobaric separation with this detector, the isobaric pair of  $^{58}$ Fe/ $^{58}$ Ni was explored at detector pressures from 20 to 55 Torr in 5 Torr steps (see Fig. 7). The cross-over point of the two isobars' Bragg Curves occurred sooner within the detector than what was predicted by Geant4. The cause for this discrepancy is unclear and



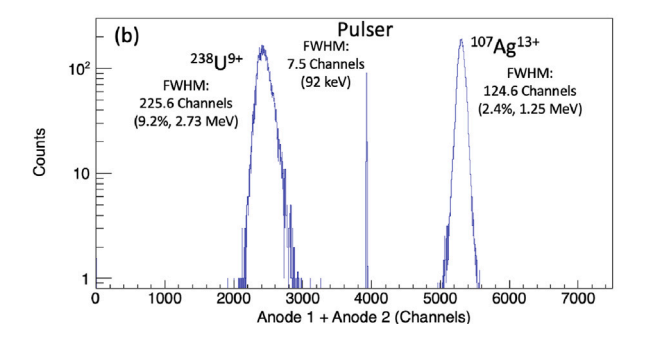


**Fig. 6.** Superposition of separate runs of a pulser,  $^{238}$ U $^{9+}$  at 44.2 MeV, and  $^{107}$ Ag $^{13+}$  at 83.3 MeV at a detector pressure of 40 Torr. Spectra (a) shows the two-dimensional energy loss plot from each of the two anodes while (b) is the one-dimensional plot of the sum of the two anodes. The projected resolution in percent was determined by the FWHM over the centroid and this was then projected into energy by using the predicted energy loss from the Geant4 simulation.

Table 1

The detector resolution by means of the full-width at half-maximum (FWHM) in channels over the centroid is presented for a subset of ions and detector pressures tested when the time-of-flight was not in use.

	Incident		Anode	Anode	
	Energy	Pressure	1	2	Sum
Ion	(MeV)	(Torr)	(%)	(%)	(%)
<sup>12</sup> C <sup>3+</sup>	13.3	40	4.4	4.0	3.3
<sup>12</sup> C <sup>5+</sup>	36.8	40	5.0	5.0	3.5
$^{28}Si^{4+}$	30.1	40	3.4	4.6	1.6
<sup>56</sup> Fe <sup>7+</sup>	46.2	40	2.3	6.4	2.2
<sup>58</sup> Fe <sup>8+</sup>	58.2	40	3.0	4.1	1.8
<sup>107</sup> Ag <sup>13+</sup>	83.3	40	2.9	4.9	2.4
109Ag13+	81.8	40	3.4	5.2	3.0
$^{238}U^{9+}$	44.2	20.8	5.4	10.4	4.9
$^{238}U^{9+}$	44.2	40	8.1	18.1	9.2

should be investigated. It may be due to an improper calibration of the gas-handling system's pressure transducer for isobutane, an unexpected pressure gradient due to the distance and constrictions of the supply and return gas lines, or discrepancy related to gas density in the simulation. In order to minimize the observed discrepancy in energy loss, a constant value of 8.5 Torr had been added to each simulation case. For example, experimental data at 25 Torr was compared to simulations of 33.5 Torr. Spectra from the adjusted simulation are presented alongside the experimental spectra in Fig. 7. Using this offset qualitatively demonstrates reasonable agreement, although deviations can be seen as pressure increases.

#### 5.2. Time-of-flight system performance

With the completion of the IC and simultaneous changes in the time-of-flight system's carbon foils, data was collected to quantify the effects on the transmission from the  $90^\circ$  MCP to the energy detector and the time-of-flight resolution. Results with the two system configurations described in Section 3.1.1 are presented in Table 2 and demonstrate

**Table 2**Transmission measurements of <sup>127</sup>I and <sup>238</sup>U as determined through ratios of the scalers of each detection system are presented. The second foil frame was 12 mm diameter when the Si was used and 18 mm diameter when the IC was used. The ToF transmission listed is the transmission between the two MCP detectors while the total transmission represents the transmission between the first MCP and the energy detector.

Ion	Incident Energy (MeV)	Energy Detector	Foil Thickness (µg/cm <sup>2</sup> )	ToF Transmission (%)	Total Transmission (%)	ToF Resolution (ns)
127 I <sup>9+</sup>	78.2	Si	10	23	21	0.87
$^{127}I^{7+}$	49.2	IC	2.9	47	29	1.37
$^{238}U^{9+}$	43.6	Si	9.6	18	4	1.15
$^{238}U^{9+}$	44.2	IC	2.9	25	20	1.30

a factor of five improvement in efficiency for uranium beams. Due to accelerator instability, iodine had to be tested at a terminal voltage of 6.1 MV instead of 7.7 MV and beam energy of 49.2 MeV instead of 78.2 MeV. Smaller systematic changes in time-of-flight conditions for comparison were made impossible due to incidents resulting in the breaking of previous carbon foils either through vacuum incidents, such as venting or pumping too rapidly, or mechanical stresses while handling the detectors.

When comparing the data for foil thickness and total transmission presented in Table 2 to Fig. 5 there is clear disagreement between the measured and simulated transmissions. We believe that this discrepancy is primarily due to a difference in the effective foil thickness compared to its listed thickness. These foils were coated in collodion to assist floating thin foils on large diameter frames. If this coating was not fully removed then it will cause additional energy straggling. Similar disagreements in the scattering distribution were observed in tests at other facilities [15,16] in which they too believed this to be the cause. The results for both the 9.6 µg/cm<sup>2</sup>, which was predicted to fall in the range of 30%–36%, and the  $3 \mu g/cm^2$  foil, which was predicted as roughly 76%, are in poor agreement with the simulation until the presence of a collodion layer is considered. The foil manufacturer suggests that this coating may have a typical areal density of  $20\pm10 \,\mu\text{g/cm}^2$  [17]. Only when this large range is added do the experimental observations reasonably agree with the simulations. This result was both surprising and encouraging as it provides a path for future improvement.

The changes within the system have also resulted in a worsening of the time-of-flight resolution. This was also predicted by the simulation, using the thicker simulated foils, yielded resolutions of 1.15 and 1.30 ns for the Si and IC configurations respectively for a 44 MeV uranium beam. This was within excellent agreement to the observed resolutions. The cause for the decrease in resolution was due to the increased diameter of the 45° foil frame which resulted in an increase in the flight path variation of the near and far ends of the foil. Fig. 8 demonstrates experimental data (a) and simulated data (b) where the simulated carbon foil thicknesses were tuned such that the one dimensional time-of-flight spectra match in resolution (1.3 ns in this case). Surprisingly, the experimental data appears to offer higher discrimination power due to an unexpected energy and time-of-flight relation. This is best explained by a relationship between the amplitude of the IC signal and the ion trajectory. As shown in Fig. 4, particles hitting the top of the 45° MCP foil will have a slightly longer timeof-flight path than those which hit the bottom. Simultaneously, ions with the longest path will enter the IC near the anodes with an upward trajectory while those with a shorter path enters near the cathode with a downward trajectory. In either case the amplitude within the IC may be position dependent if the Frisch grid does not sufficiently remove this effect. Alternatively, the ions nearest the cathode may have their electron avalanche partially absorbed or even hit the cathode plate directly. Visualizations by Geant4 suggest the latter should occur with a small, but non-zero, probability. These observations encouraged further exploration of system parameters within the simulation.

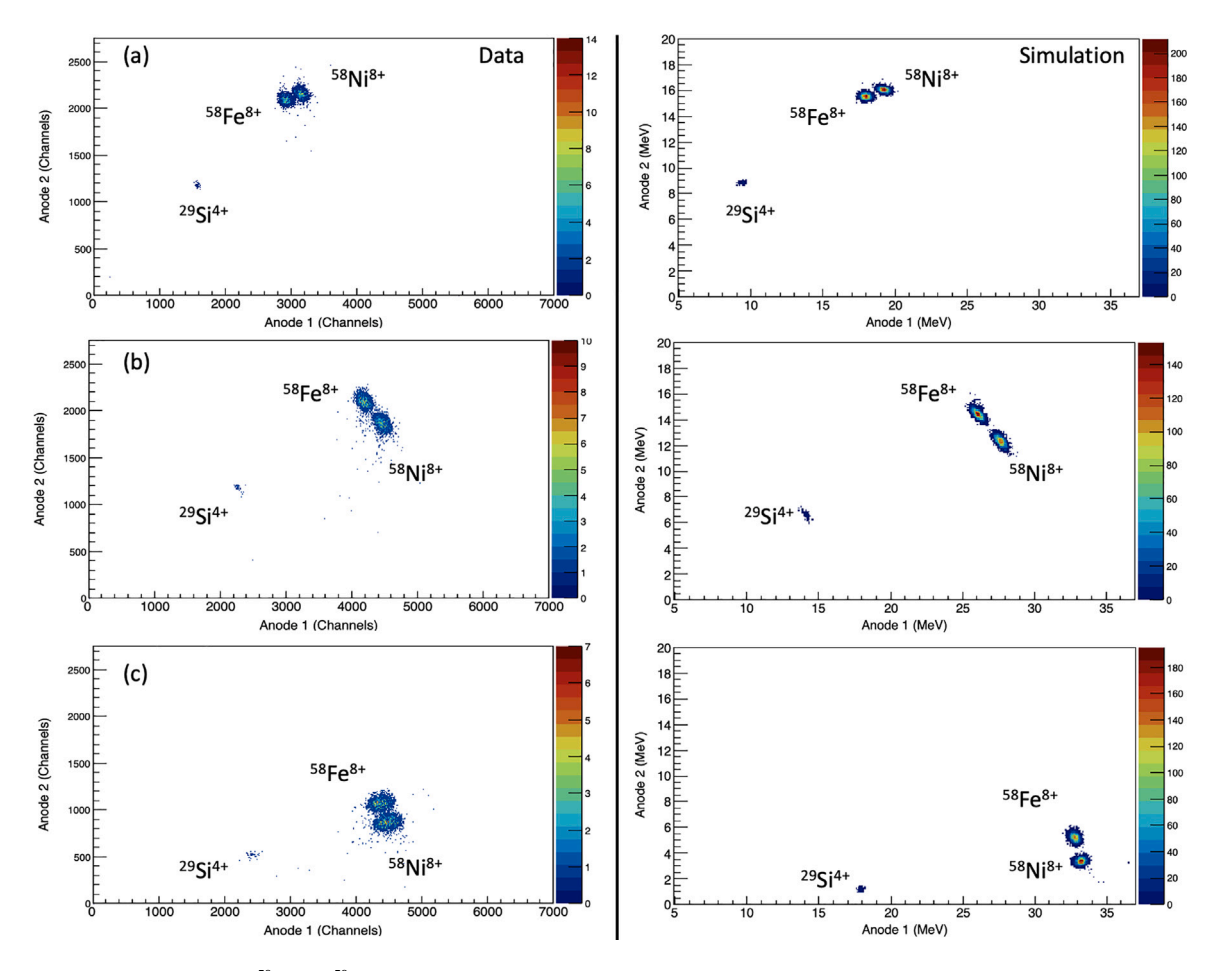


Fig. 7. The relative isobaric separation of <sup>58</sup>Fe and <sup>58</sup>Ni at a detector pressure of (a) 25 Torr (b) 40 Torr and (c) 55 Torr where experimental data is shown on the left and simulation is shown on the right. The number of simulated ions for each species was scaled to match the composition seen in the data. All simulated pressures used within this comparison were 8.5 Torr higher than the transducer pressure recorded during testing. This was based off discrepancies in energy losses as described in the text.

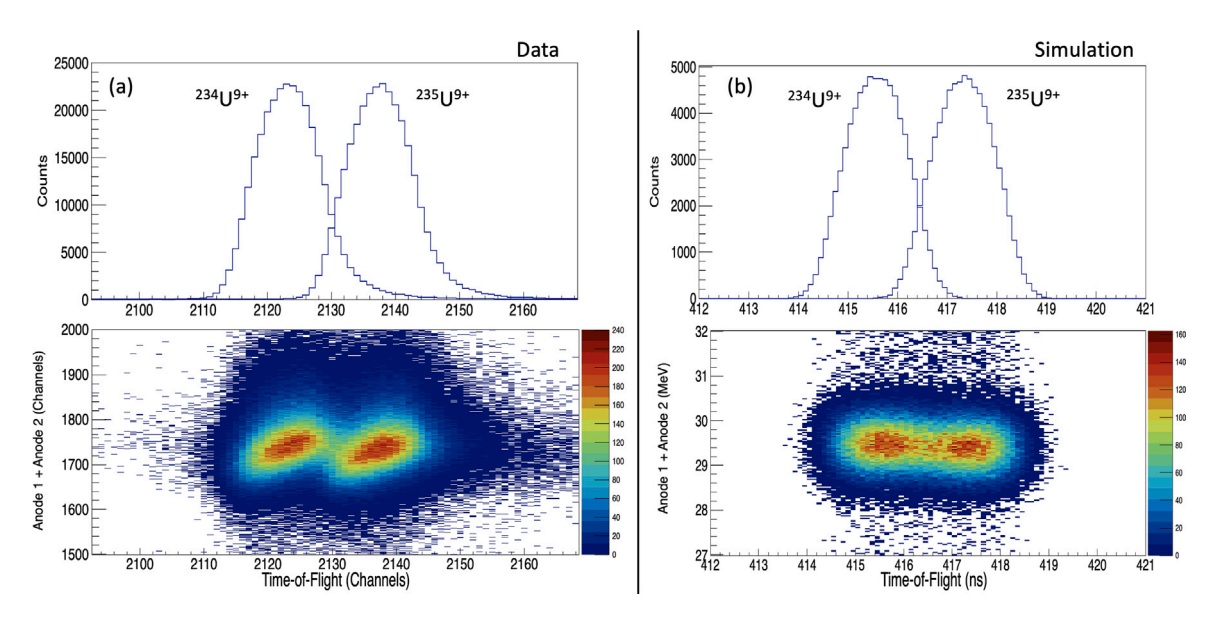


Fig. 8. Data (left) and simulation (right) for the cases of  $^{234}$ U and  $^{235}$ U to demonstrate nearby mass discrimination offered by the detector system as described with the IC as the energy detector.

By exploring foil thicknesses in the simulation, it is predicted that with the present foils, the resolution could be improved to 1 ns or better, while simultaneously having a minimal impact on the transmission, by having the  $45^\circ$  MCP come first. This improvement, however, will

still vary with beam size at the 45° foil frame. Alternatively, the 45° MCP could be replaced or converted into a second 90° configuration which is predicted to improve both transmission and resolution. Projecting these improvements for  $^{129}\text{I}$  measurements, we estimate that

the overall detection efficiency for a 78.2~MeV iodine beam would improve from 21% to 54%; however, this will need to be experimentally verified.

#### 6. Conclusions and future work

The implementation of thinner carbon foils, a larger diameter frame for the 45° MCP, and the larger acceptance of the new compact IC resulted in an increased detection efficiency from 4% to 20% for a 44 MeV uranium beam. The largest improvement was attributed to the size of the IC detector window. This was made clear since observed transmission between the MCPs alone improved from 18% to 25% as a result of the thinner foils and the larger 45° MCP frame.

For future developments, we plan to avoid using foils with collodion and accept the increased difficulty in floating since it is beneficial for foils to be as thin as possible. Additionally, it has been shown that many facilities use ultra-thin diamond-like foils as thin as 0.5 µg/cm<sup>2</sup> [18]. These foils, however, have an additional transmission loss since a support grid is required. Our simulation indicates that a non-coated  $3 \mu g/cm^2$  foil with no support grid should produce a similar overall efficiency as if one diamond-like foil with 75% transparency is used and is higher if two are used. However, since the time-of-flight resolution improves as a function of foil thickness, the diamond-like foils should offer superior discrimination capabilities when used as the first foil within the system. For future improvements of the time-of-flight system's resolution, the described Geant4 simulation predicted that the order of the two different MCP designs should be reversed or the  $45^{\circ}$ design should be reconfigured into an additional 90° design, as used at other facilities [19].

As described in Section 2, the initial commissioning and testing of the compact IC was performed with a detector window that deviated from the original design. Despite this, the detector resolution was still found to be sufficient for our applications. This detector has added versatility by providing additional energy loss information, demonstrated through the identification of <sup>58</sup>Fe and <sup>58</sup>Ni isobars, and increased resistance to higher beam currents and masses. Continued effort toward obtaining a leak tight window using the recessed window mount is expected to further improve the energy resolution. Based on the encouraging results of the energy resolution and observed improvements in detection efficiency, these upgrades are expected to allow for measurements of <sup>236</sup>U in natural uranium ore materials as well as improve our capabilities for environmental <sup>129</sup>I measurements.

## CRediT authorship contribution statement

Adam M. Clark: Conceptualization, Methodology, Software, Validation, Formal analysis, Investigation, Writing – original draft, Visualization. Austin D. Nelson: Conceptualization, Methodology, Validation, Investigation, Writing – review & editing. Thomas L. Bailey: Methodology, Validation, Investigation, Writing – review & editing. Lauren K. Callahan: Investigation, Writing – review & editing. Adam Mazurek: Investigation, Writing – review & editing. Philippe Collon: Conceptualization, Methodology, Writing – review & editing, Supervision, Project administration, Funding acquisition.

## Declaration of competing interest

The authors declare that they have no known competing financial interests or personal relationships that could have appeared to influence the work reported in this paper.

## Data availability

Data will be made available on request.

#### Acknowledgments

We would like to thank Dr. Martin Martschini for providing CAD drawings, electrical diagrams, and a spare pre-amp board of the ANU detector as well as Prof. Michael Paul for loaning both MCP detectors for this work. We would also like to thank Jerry Lingle of the NSL who assisted in the planning and manufacturing of key components for the compact detector, as well as Jim Kaiser of the NSL who constructed and planned the additional electrical work required for the actuation and safety interlocks for the detector as well as the creation of the inhouse NIM module which adapted the output signals from the detector system. This work is supported by the National Science Foundation under Grant No. PHY-2011890 and the Nuclear Regulatory Commission award 31310019M0037.

#### References

- M. Yamamoto, Y. Yamauchi, K. Chatani, S. Igarashi, K. Komura, K. Ueno, M. Sakanoue, Distribution of global fallout Np-237, Pu isotopes, and Am-241 in lake and sea sediments, J. Radioanal. Nucl. Chem. 147 (1) (1991) 165–176, http://dx.doi.org/10.1007/BF02039578.
- [2] A. Sakaguchi, K. Kawai, P. Steier, F. Quinto, K. Mino, J. Tomita, M. Hoshi, N. Whitehead, M. Yamamoto, First results on <sup>236</sup>U levels in global fallout, Sci. Total Environ. 407 (14) (2009) 4238–4242, http://dx.doi.org/10.1016/j. scitotenv.2009.01.058.
- [3] M. Castrillejo, N. Casacuberta, M. Christl, J. Garcia-Orellana, C. Vockenhuber, H.-A. Synal, P. Masqué, Anthropogenic <sup>236</sup>U and <sup>129</sup>I in the Mediterranean Sea: First comprehensive distribution and constrain of their sources, Sci. Total Environ. 593–594 (2017) 745–759, http://dx.doi.org/10.1016/j.scitotenv.2017.03.201.
- [4] K. Hain, P. Steier, M.B. Froehlich, R. Golser, X. Hou, J. Lachner, T. Nomura, J. Qiao, F. Quinto, A. Sakaguchi, <sup>233</sup>U/<sup>236</sup>U signature allows to distinguish environmental emissions of civil nuclear industry from weapons fallout, Nat. Commun. 11 (1) (2020) 1275, http://dx.doi.org/10.1038/s41467-020-15008-2.
- [5] A. Wallner, M. Froehlich, M. Hotchkis, N. Kinoshita, M. Paul, M. Martschini, S. Pavetich, S. Tims, N. Kivel, D. Schumann, M. Honda, H. Matsuzaki, T. Yamagata, <sup>60</sup>Fe and <sup>244</sup>Pu deposited on Earth constrain the r-process yields of recent nearby supernovae, Science 372 (6543) (2021) 742, http://dx.doi.org/10.1126/science.aax3972.
- [6] X. Wang, A.M. Clark, J. Ellis, A.F. Ertel, B.D. Fields, B.J. Fry, Z. Liu, J.A. Miller, R. Surman, r-process Radioisotopes from Near-Earth Supernovae and Kilonovae, Astrophys. J. 923 (2021) http://dx.doi.org/10.3847/1538-4357/ac2d90.
- [7] M. Skulski, T. Anderson, L. Callahan, A.M. Clark, A.D. Nelson, D. Robertson, E. Stech, P. Collon, Recent developments in the AMS system at the Nuclear Science Laboratory: Impacts on radionuclide sensitivities and current capabilities, Nucl. Instrum. Methods Phys. Res. B 488 (2021) 30–36, http://dx.doi.org/10.1016/j.nimb.2020.12.009.
- [8] M.A. Skulski Jr., Development of <sup>129</sup>I AMS at the Nuclear Science Laboratory for Measurements of the Great Lakes Region (Ph.D. thesis), University of Notre Dame, 2020.
- [9] M. Stocker, M. Döbeli, M. Grajcar, M. Suter, H.-A. Synal, L. Wacker, A universal and competitive compact AMS facility, Nucl. Instrum. Methods Phys. Res. B 240 (1) (2005) 483–489, http://dx.doi.org/10.1016/j.nimb.2005.06.224.
- [10] O. Forstner, L. Michlmayr, M. Auer, R. Golser, W. Kutschera, A. Priller, P. Steier, A. Wallner, Applications of a compact ionization chamber in AMS at energies below 1MeV/amu, Nucl. Instrum. Methods Phys. Res. B 266 (10) (2008) 2213–2216, http://dx.doi.org/10.1016/j.nimb.2008.02.060.
- [11] M. Martschini, L.K. Fifield, M.B. Froehlich, G. Leckenby, S. Pavetich, S.G. Tims, B. Tranter, A. Wallner, New and upgraded ionization chambers for AMS at the Australian National University, Nucl. Instrum. Methods Phys. Res. B 438 (2019) 141–147, http://dx.doi.org/10.1016/j.nimb.2018.05.039.
- [12] D. Berkovits, H. Feldstein, S. Ghelberg, A. Hershkowitz, E. Navon, M. Paul, <sup>236</sup>U in uranium minerals and standards, Nucl. Instrum. Methods Phys. Res. B 172 (1) (2000) 372–376, http://dx.doi.org/10.1016/S0168-583X(00)00152-X.
- [13] L. Zheng, H. Matsuzaki, T. Yamagata, A comparison between Geant4 simulation and experiment for time-of-flight measurement, Appl. Phys. Express 15 (8) (2022) 084007, http://dx.doi.org/10.35848/1882-0786/ac8413.
- [14] J.O. Stoner, Densities of carbon foils, Nucl. Instrum. Methods Phys. Res. A 303
   (1) (1991) 94–98, http://dx.doi.org/10.1016/0168-9002(91)90769-M.
- [15] P. Steier, Exploring the Limits of VERA: A Universal Facility for Accelerator Mass Spectrometry (Ph.D. thesis), University of Vienna, 2020.
- [16] L.G. Gladkis, Development of AMS Techniques for <sup>53</sup>Mn and <sup>236</sup>U (Ph.D. thesis), Australia National University, 2006.
- [17] Arizona Carbon Foil Co. Inc., Product information, 2020, URL https://www.acf-metals.com/product-information.

- [18] V. Liechtenstein, T. Ivkova, E. Olshanski, R. Golser, W. Kutschera, P. Steier, C. Vockenhuber, R. Repnow, R. von Hahn, M. Friedrich, U. Kreissig, Recent investigations and applications of thin diamond-like carbon (DLC) foils, Nucl. Instrum. Methods Phys. Res. A 521 (1) (2004) 197–202, http://dx.doi.org/10.1016/j.nima.2003.11.151.
- [19] C. Vockenhuber, I. Ahmad, R. Golser, W. Kutschera, V. Liechtenstein, A. Priller, P. Steier, S. Winkler, Accelerator mass spectrometry of heavy long-lived radionuclides, Int. J. Mass Spectrom. 223–224 (2003) 713–732, http://dx.doi.org/10.1016/S1387-3806(02)00944-2.